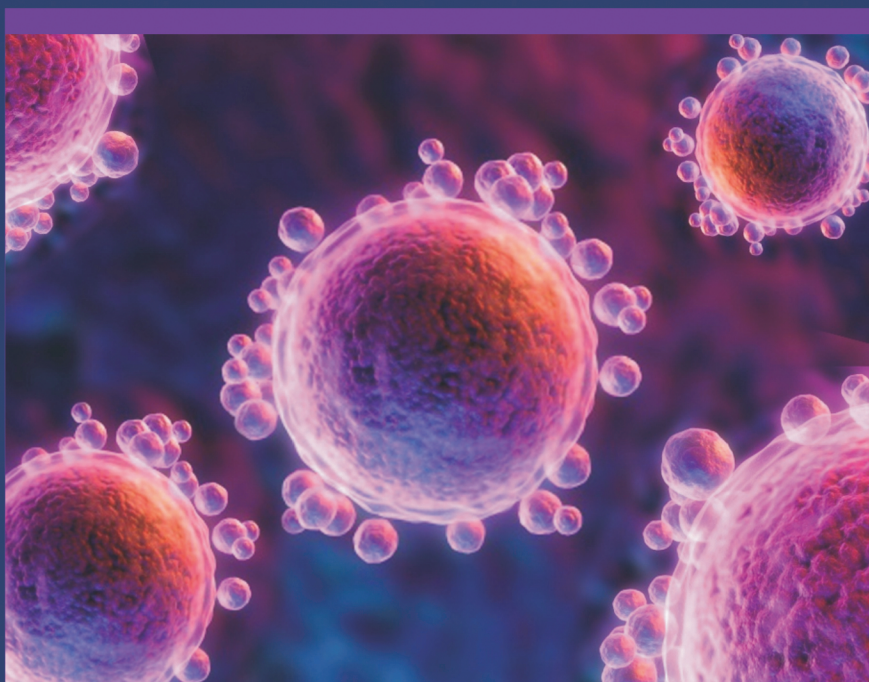


Trends in

BIOPHYSICS

From Cell Dynamics Toward Multicellular Growth Phenomena



Pavel Kraikivski, PhD
Editor



Apple Academic Press



CRC Press
Taylor & Francis Group

TRENDS IN BIOPHYSICS

From Cell Dynamics Toward
Multicellular Growth Phenomena

TRENDS IN BIOPHYSICS

From Cell Dynamics Toward
Multicellular Growth Phenomena

Edited by
Pavel Kraikivski, PhD



Apple Academic Press

TORONTO NEW JERSEY

CRC Press
Taylor & Francis Group
6000 Broken Sound Parkway NW, Suite 300
Boca Raton, FL 33487-2742

Apple Academic Press, Inc
3333 Mistwell Crescent
Oakville, ON L6L 0A2
Canada

© 2013 by Apple Academic Press, Inc.

Exclusive worldwide distribution by CRC Press an imprint of Taylor & Francis Group, an Informa business

No claim to original U.S. Government works
Version Date: 20130401

International Standard Book Number-13: 978-1-4665-8410-5 (eBook - PDF)

This book contains information obtained from authentic and highly regarded sources. Reasonable efforts have been made to publish reliable data and information, but the author and publisher cannot assume responsibility for the validity of all materials or the consequences of their use. The authors and publishers have attempted to trace the copyright holders of all material reproduced in this publication and apologize to copyright holders if permission to publish in this form has not been obtained. If any copyright material has not been acknowledged please write and let us know so we may rectify in any future reprint.

Except as permitted under U.S. Copyright Law, no part of this book may be reprinted, reproduced, transmitted, or utilized in any form by any electronic, mechanical, or other means, now known or hereafter invented, including photocopying, microfilming, and recording, or in any information storage or retrieval system, without written permission from the publishers.

For permission to photocopy or use material electronically from this work, please access www.copyright.com (<http://www.copyright.com/>) or contact the Copyright Clearance Center, Inc. (CCC), 222 Rosewood Drive, Danvers, MA 01923, 978-750-8400. CCC is a not-for-profit organization that provides licenses and registration for a variety of users. For organizations that have been granted a photocopy license by the CCC, a separate system of payment has been arranged.

Trademark Notice: Product or corporate names may be trademarks or registered trademarks, and are used only for identification and explanation without intent to infringe.

Visit the Taylor & Francis Web site at
<http://www.taylorandfrancis.com>

and the CRC Press Web site at
<http://www.crcpress.com>

For information about Apple Academic Press product
<http://www.appleacademicpress.com>

About the Editor

Pavel Kraikivski, PhD

Pavel Kraikivski, PhD, is a research faculty member in the Department of Biological Sciences at Virginia Polytechnic Institute and State University, Blacksburg, Virginia, USA. He has acted as a reviewer for several journals and has several published articles to his name as well as several presentations at professional meetings. His current research interests include biophysics, system biology, molecular biophysics and structural biology, cell cycles, intracellular systems, and intracellular transport.

Dr. Kraikivski has a unique academic background from his education at Russian, German, and American universities and an extensive scientific research education. He has conducted research at the Max-Planck Institute for Colloids and Interfaces in Germany, where his research focused on active bio-polymers, and has also worked at the Center for Cell Analysis and Modeling at the University of Connecticut Health Center. He has made significant contributions in computational cell biology and biophysics, particularly in the areas of intracellular transport and cytoskeleton dynamics.

Contents

<i>List of Contributors</i>	<i>ix</i>
<i>List of Abbreviations</i>	<i>xiii</i>
<i>Introduction</i>	<i>xv</i>
1. Mammalian Cell Cycle Regulation	1
Rajat Singhanian, R. Michael Sramkoski, James W. Jacobberger, and John J. Tyson	
2. Spindles and Active Vortices	25
David A. Head, W. J. Briels, and Gerhard Gompper	
3. Actomyosin-Dependent Cortical Dynamics	49
Patrizia Sommi, Dhanya Cheerambathur, Ingrid Brust-Mascher, and Alex Mogilner	
4. Filament Depolymerization During Bacterial Mitosis	71
Edward J. Banigan, Michael A. Gelbart, Zemer Gitai, Ned S. Wingreen, and Andrea J. Liu	
5. Actin Ring Constriction	95
Alexander Zumdieck, Karsten Kruse, Henrik Bringmann, Anthony A. Hyman, and Frank Jülicher	
6. Curved Activators and Cell-Membrane Waves	109
Barak Peleg, Andrea Disanza, Giorgio Scita, and Nir Gov	
7. Actin Waves and Phagocytic Cup Structures	133
Günther Gerisch	
8. Yeast and Scaling	145
Daniel Riveline	
9. Cellular Shapes from Protrusive and Adhesive Forces	157
Roie Shlomovitz, Kathrin Schloen, Theresia Stradal, and Nir S. Gov	
10. Amoeboid Cells' Protrusions	193
Peter J. M. Van Haastert	
11. Collective Cell Migration	205
Masataka Yamao, Honda Naoki, and Shin Ishii	

12. Differential Adhesion and Cell Sorting..... 237
Ying Zhang, Gilberto L. Thomas, Maciej Swat, Abbas Shirinifard,
and James A. Glazier

Author Notes 263

Index 269

List of Contributors

Edward J. Banigan

Department of Physics and Astronomy, University of Pennsylvania, Philadelphia, Pennsylvania, United States of America

W. J. Briels

Computational Biophysics, University of Twente, 7500 AE Enschede, The Netherlands

Henrik Bringmann

Max Planck Institute for Molecular Cell Biology and Genetics, Dresden, Germany

Ingrid Brust-Mascher

Department of Molecular and Cellular Biology, University of California Davis, Davis, California, United States of America

Dhanya Cheerambathur

Department of Cellular and Molecular Medicine, Ludwig Institute for Cancer Research, University of California San Diego, La Jolla, California, United States of America

Andrea Disanza

IFOM, the FIRC Institute for Molecular Oncology Foundation, Milan, Italy

Michael A. Gelbart

Graduate Program in Biophysics, Harvard University, Boston, Massachusetts, United States of America, Department of Physics, Princeton University, Princeton, New Jersey, United States of America

Günther Gerisch

Max-Planck-Institut für Biochemie, D-82152 Martinsried, Germany

Zemer Gitai

Department of Molecular Biology, Princeton University, Princeton, New Jersey, United States of America

James A. Glazier

Biocomplexity Institute and Department of Physics, Indiana University, Bloomington, Indiana, United States of America

Gerhard Gompper

Theoretical Soft Matter and Biophysics, Institute of Complex Systems, Forschungszentrum Jülich, 52425 Jülich, Germany

Nir S. Gov

Department of Chemical Physics, The Weizmann Institute of Science, Rehovot, Israel

David A. Head

Theoretical Soft Matter and Biophysics, Institute of Complex Systems, Forschungszentrum Jülich, 52425 Jülich, Germany; Computational Biophysics, University of Twente, 7500 AE Enschede, The Netherlands; School of Computing, Leeds University, Leeds LS2 9JT, UK

Anthony A. Hyman

Max Planck Institute for Molecular Cell Biology and Genetics, Dresden, Germany

Shin Ishii

Graduate School of Informatics, Kyoto University, Uji, Kyoto, Japan; RIKEN Computational Science Research Program, Wako, Saitama, Japan

James W. Jacobberger

Case Comprehensive Cancer Center, Case Western Reserve University, Cleveland, Ohio, United States of America

Frank Jülicher

Max Planck Institute for the Physics of Complex Systems, Dresden, Germany

Doron Kabaso

Department of Chemical Physics, The Weizmann Institute of Science, Rehovot, Israel

Karsten Kruse

Max Planck Institute for the Physics of Complex Systems, Dresden, Germany

Andrea J. Liu

Department of Physics and Astronomy, University of Pennsylvania, Philadelphia, Pennsylvania, United States of America

Alex Mogilner

Department of Neurobiology, Physiology and Behavior, University of California Davis, Davis, California, United States of America; Department of Mathematics, University of California Davis, Davis, California, United States of America

Honda Naoki

Graduate School of Informatics, Kyoto University, Uji, Kyoto, Japan

Barak Peleg

Department of Chemical Physics, the Weizmann Institute of Science, Rehovot, Israel

Daniel Riveline

Laboratory of Yeast Genetics and Cell Biology, The Rockefeller University, New York, New York, United States of America; Laboratoire de Spectrométrie Physique (CNRS), UMR 5588, Université Joseph Fourier, Saint-Martin d'Hères, France

Kathrin Schloen

Helmholtz Center for Infection Research, Braunschweig, Germany

Giorgio Scita

IFOM, the FIRC Institute for Molecular Oncology Foundation, Milan, Italy, Department of Medicine, Surgery and Dentistry, Università degli Studi di Milano, Milan, Italy

Abbas Shirinifard

Biocomplexity Institute and Department of Physics, Indiana University, Bloomington, Indiana, United States of America

Roie Shlomovitz

Department of Chemical Physics, The Weizmann Institute of Science, Rehovot, Israel

Rajat Singhania

Department of Biological Sciences, Virginia Polytechnic Institute and State University, Blacksburg, Virginia, United States of America

Patrizia Sommi

Human Physiology Section, Department of Physiology, University of Pavia, Pavia, Italy

R. Michael Sramkoski

Case Comprehensive Cancer Center, Case Western Reserve University, Cleveland, Ohio, United States of America

Maciej Swat

Biocomplexity Institute and Department of Physics, Indiana University, Bloomington, Indiana, United States of America

Theresia Stradal

Helmholtz Center for Infection Research, Braunschweig, Germany

Gilberto L. Thomas

Instituto de Física, Universidade Federal do Rio Grande do Sul, Porto Alegre, Brazil

John J. Tyson

Department of Biological Sciences, Virginia Polytechnic Institute and State University, Blacksburg, Virginia, United States of America

Ned S. Wingreen

Department of Molecular Biology, Princeton University, Princeton, New Jersey, United States of America

Masataka Yamao

Graduate School of Information Science, Nara Institute of Science and Technology, Ikoma, Nara, Japan

Ying Zhang

Cancer and Developmental Biology Laboratory, National Cancer Institute, Frederick, Maryland, United States of America

Alexander Zumdieck

Max Planck Institute for the Physics of Complex Systems, Dresden, Germany

List of Abbreviations

ADF	Actin depolymerizing factor
AFM	Atomic force microscopy
APC-C	Anaphase Promoting Complex-Cyclosome
ATPase	Adenosine triphosphate
BAR	Bin/Amphiphysin/Rvs
BNs	Boolean networks
BSA	Bovine serum albumin
cAMP	Cyclic adenosine monophosphate
CAM	Cell adhesion molecule
CDM	Cis-dimer model
CDR	Circular Dorsal Ruffles
DAH	Differential Adhesion Hypothesis
DAPI	4',6-diamidino-2-phenylindole
DMEM	Dulbecco's modified minimal essential media
DMSO	Dimethyl sulfoxide
DNA	Deoxyribonucleic acid
DROK	Drosophila Rho-associated kinase
EB1	End binding protein
ECM	Extra-cellular matrix
EGM-2	Endothelial Cell Growth Medium-2
EST	Expressed sequence tag
FBS	Fetal bovine serum
FCS	Fetal calf serum
FITC	Fluorescein isothiocyanate
GEF	Guanine nucleotide exchange factors
GFP	Green fluorescent protein
GGH	Glazier-Graner-Hogeweg
GTP	Guanosine 5'-triphosphate
HBL	Heterotypic boundary length
HUVEC	Human Umbilical Vein Endothelial Cell
IMD	IRSp53-Missing-In-Metastasis domains
IRSp53	Insulin receptor substrate protein of 53 kDa
LZM	Linear-zipper model
MCS	Monte Carlo Step
MEF	Mouse embryonic fibroblasts
MIM	Missing-in-metastasis
MLC	Myosin light chain
mRFP	Monomeric red fluorescent protein
MT	Microtubule
NEB	Nuclear envelope breakdown
NETO	New End Take-Off

N-WASP	Neural Wiskott-Aldrich syndrome protein
NWHBL	Normalized weighted heterotypic boundary length
ODEs	Ordinary differential equations
PB	Phosphate buffer
PBS	Phosphate buffered saline
PDGF	Platelet-derived growth factor
PFA	Paraformaldehyde
PIP3	Phosphatidylinositol (3,4,5)-triphosphate
PV	Pressure-volume
RKO	Human colorectal carcinoma
RNAi	Ribonucleic acid interference
Sced	Staphylococcus epidermidis
SCF	Skp, Cullin, F-box
SD	Standard deviation
SM	Saturation model
SMC	Structural maintenance of chromosomes
TF	Transcription factors
THBM	Trans-homophilic-bond model
TIRF	Total internal reflection fluorescence
WGA	Wheat germ agglutinin
WHBL	Weighted heterotypic boundary length
WT	Wild-type

Introduction

The physiological behaviors of cells (growth and division, differentiation, movement, death, etc.) are controlled by complex networks of interacting genes and proteins, and a fundamental goal of computational cell biology is to develop dynamical models of these regulatory networks that are realistic, accurate and predictive. Historically, these models have divided along two basic lines: deterministic or stochastic, and continuous or discrete, with scattered efforts to develop hybrid approaches that bridge these divides.

In chapter 1 of this volume, using the cell cycle control system in eukaryotes as an example, Singhanian and colleagues propose a hybrid approach that combines a continuous representation of slowly changing protein concentrations with a discrete representation of components that switch rapidly between “on” and “off” states, combining the deterministic causality of network interactions with the stochastic uncertainty of random events. The hybrid approach can be easily tailored to the available knowledge of control systems, and it provides both qualitative and quantitative results that can be compared to experimental data to test the accuracy and predictive power of the model.

In chapter 2, Head, Briels, and Gompper present the results of numerical simulations of a discrete filament-motor protein model confined to a pressurized cylindrical box. Stable spindles, nematic configurations, asters, and high-density semi-asters spontaneously emerge. State diagrams are presented delineating each stationary state as the pressure, motor speed and motor density are varied. The authors further highlight a parameter regime where vortices form exhibiting collective rotation of all filaments, but have a finite lifetime before contracting to a semi-aster. They demonstrate that discrete filament-motor protein models provide new insights into the stationary and dynamical behavior of active gels and subcellular structures, because many phenomena occur on the length-scale of single filaments.

In yet another scenario, the assembly of the *Drosophila* embryo mitotic spindle during prophase depends upon a balance of outward forces generated by cortical dynein and inward forces generated by kinesin-14 and nuclear elasticity. Myosin II is known to contribute to the dynamics of the cell cortex but how this influences the prophase force-balance is unclear. Sommi and her colleagues investigate this question in chapter 3; they did so by injecting the myosin II inhibitor, Y27632, into early *Drosophila* embryos. They observed a significant increase in both the area of the dense cortical actin caps and in the spacing of the spindle poles. Their results suggest that two complementary outward forces are exerted on the prophase spindle by the overlying cortex. Specifically, dynein localized on the mechanically firm actin caps and the actomyosin-driven contraction of the deformable soft patches of the actin cortex, cooperate to pull astral microtubules outward. Thus, myosin II controls the size and dynamic properties of the actin-based cortex to influence the spacing of the poles of the underlying spindle during prophase.

Reliable chromosome segregation is crucial to all dividing cells. In some bacteria, segregation has been found to occur in a rather counterintuitive way: the chromosome attaches to a filament bundle and erodes it by causing depolymerization of the filaments. Moreover, unlike eukaryotic cells, bacteria do not use molecular motors and/or macromolecular tethers to position their chromosomes. This raises the general question of how depolymerizing filaments alone can continuously and robustly pull cargo as the filaments themselves are falling apart. In chapter 4, Banigan and his colleagues introduce the first quantitative physical model for depolymerization-driven translocation in a many-filament system. Their simulations of this model suggest a novel underlying mechanism for robust translocation, namely self-diffusiophoresis, motion of an object in a self-generated concentration gradient in a viscous environment. In this case, the cargo generates and sustains a concentration gradient of filaments by inducing them to depolymerize. The authors demonstrate that their model agrees well with existing experimental observations such as segregation failure, filament-length-dependent translocation velocity, and chromosomal compaction. In addition, they make several predictions—including predictions for the specific modes by which the chromosome binds to the filament structure and triggers its disassembly—that can be tested experimentally.

Next, in chapter 5, Zumdick and his coauthors present a physical analysis of the dynamics and mechanics of contractile actin rings. In particular, they analyze the dynamics of ring contraction during cytokinesis in the *Caenorhabditis elegans* embryo. They present a general analysis of force balances and material exchange and estimate the relevant parameter values. The authors show that on a microscopic level contractile stresses can result from both the action of motor proteins, which cross-link filaments, and from the polymerization and depolymerization of filaments in the presence of end-tracking cross-linkers.

In chapter 6 we turn our attention to cells that exhibit propagating membrane waves which involve the actin cytoskeleton. One type of such membranal waves are Circular Dorsal Ruffles (CDR), which are related to endocytosis and receptor internalization. Experimentally, CDRs have been associated with membrane bound activators of actin polymerization of concave shape. Peleg and colleagues present experimental evidence for the localization of convex membrane proteins in these structures, and their insensitivity to inhibition of myosin II contractility in immortalized mouse embryo fibroblasts cell cultures. These observations lead the authors to propose a theoretical model that explains the formation of these waves due to the interplay between complexes that contain activators of actin polymerization and membrane-bound curved proteins of both types of curvature (concave and convex). Their model predicts that the activity of both types of curved proteins is essential for sustaining propagating waves, which are abolished when one type of curved activator is removed. Within this model waves are initiated when the level of actin polymerization induced by the curved activators is higher than some threshold value, which allows the cell to control CDR formation. The authors demonstrate that the model can explain many features of CDRs, and give several testable predictions. This chapter demonstrates the importance of curved membrane proteins in organizing the actin cytoskeleton and cell shape.

Chapter 7 deals with actin waves that are spontaneously generated on the planar, substrate-attached surface of *Dictyostelium* cells. Gerisch reveals that the waves have the following characteristics:

1. They are circular structures of varying shape, capable of changing the direction of propagation.
2. The waves propagate by treadmilling with a recovery of actin incorporation after photobleaching of less than 10 seconds.
3. The waves are associated with actin-binding proteins in an ordered 3-dimensional organization: with myosin-IB at the front and close to the membrane, the Arp2/3 complex throughout the wave, and coronin at the cytoplasmic face and back of the wave. Coronin is a marker of disassembling actin structures.
4. The waves separate two areas of the cell cortex that differ in actin structure and phosphoinositide composition of the membrane. The waves arise at the border of membrane areas rich in phosphatidylinositol (3,4,5) trisphosphate (PIP3). The inhibition of PIP3 synthesis reversibly inhibits wave formation.
5. The actin wave and PIP3 patterns resemble 2-dimensional projections of phagocytic cups, suggesting that they are involved in the scanning of surfaces for particles to be taken up.

Lengths and shapes are approached in different ways in different fields: they serve as a read-out for classifying genes or proteins in cell biology, whereas they result from scaling arguments in condensed matter physics. In chapter 8, Riveline proposes a combined approach with examples illustrated for the fission yeast *Schizosaccharomyces pombe*.

Cells have highly varied and dynamic shapes, which are determined by internal forces generated by the cytoskeleton. These forces include protrusive forces due to the formation of new internal fibers and forces produced due to attachment of the cell to an external substrate. A longstanding challenge is to explain how the myriad components of the cytoskeleton self-organize to form the observed shapes of cells. In chapter 9, Kabaso and coauthors present a theoretical study of the shapes of cells that are driven only by protrusive forces of two types; one is the force due to polymerization of actin filaments, which acts as an internal pressure on the membrane, and the second is the force due to adhesion between the membrane and external substrate. The key property is that both forces are localized on the cell membrane by protein complexes that have convex spontaneous curvature. This leads to a positive feedback that destabilizes the uniform cell shape and induces the spontaneous formation of patterns. The authors compare the resulting patterns to observed cellular shapes and find good agreement, which allows them to explain some of the puzzling dependencies of cell shapes on the properties of the surrounding matrix.

Chapter 10 deals with amoeboid cells, which crawl using pseudopods, convex extensions of the cell surface. In many laboratory experiments, cells move on a smooth substrate, but in the wild cells may experience obstacles of other cells or dead material, or may even move in liquid. To understand how cells cope with heterogeneous environments, Van Haastert has investigated the pseudopod life cycle of wild type and mutant cells moving on a substrate and when suspended in liquid. He shows that

the same pseudopod cycle can provide three types of movement that he addresses as walking, gliding and swimming. In walking, the extending pseudopod will adhere firmly to the substrate, which allows cells to generate forces to bypass obstacles. Mutant cells with compromised adhesion can move much faster than wild type cells on a smooth substrate (gliding), but cannot move effectively against obstacles that provide resistance. In a liquid, when swimming, the extending pseudopods convert to side-bumps that move rapidly to the rear of the cells. Calculations suggest that these bumps provide sufficient drag force to mediate the observed forward swimming of the cell.

During development, the formation of biological networks (such as organs and neuronal networks) is controlled by multicellular transportation phenomena based on cell migration. In multi-cellular systems, cellular locomotion is restricted by physical interactions with other cells in a crowded space, similar to passengers pushing others out of their way on a packed train. The motion of individual cells is intrinsically stochastic and may be viewed as a type of random walk. However, this walk takes place in a noisy environment because the cell interacts with its randomly moving neighbors. Despite this randomness and complexity, development is highly orchestrated and precisely regulated, following genetic (and even epigenetic) blueprints. Although individual cell migration has long been studied, the manner in which stochasticity affects multi-cellular transportation within the precisely controlled process of development remains largely unknown. To explore the general principles underlying multicellular migration, in chapter 11, the authors focus on the migration of neural crest cells, which migrate collectively and form streams. Yamao, Naoki, and Ishii introduce a mechanical model of multi-cellular migration. Simulations based on the model show that the migration mode depends on the relative strengths of the noise from migratory and non-migratory cells. Strong noise from migratory cells and weak noise from surrounding cells causes “collective migration,” whereas strong noise from non-migratory cells causes “dispersive migration.” Moreover, the authors’ theoretical analyses reveal that migratory cells attract each other over long distances, even without direct mechanical contacts. This effective interaction depends on the stochasticity of the migratory and non-migratory cells. On the basis of these findings, the authors propose that stochastic behavior at the single-cell level works effectively and precisely to achieve collective migration in multi-cellular systems.

The actions of cell adhesion molecules, in particular, cadherins during embryonic development and morphogenesis more generally, regulate many aspects of cellular interactions, regulation and signaling. Often, a gradient of cadherin expression levels drives collective and relative cell motions generating macroscopic cell sorting. Computer simulations of cell sorting have focused on the interactions of cells with only a few discrete adhesion levels between cells, ignoring biologically observed continuous variations in expression levels and possible nonlinearities in molecular binding. In the final chapter, the authors present three models relating the surface density of cadherins to the net intercellular adhesion and interfacial tension for both discrete and continuous levels of cadherin expression. Zhang and colleagues then use the Glazier-Graner-Hogeweg (GGH) model to investigate how variations in the distribution of the number of cadherins per cell and in the choice of binding model affect cell sorting. They find that an aggregate with a continuous variation in the level of a single type

of cadherin molecule sorts more slowly than one with two levels. The rate of sorting increases strongly with the interfacial tension, which depends both on the maximum difference in number of cadherins per cell and on the binding model. The authors' approach helps connect signaling at the molecular level to tissue-level morphogenesis, thus adding to our understanding of how biophysics relates to yet another realm of investigation.

— **Pavel Kraikivski, PhD**

1 Mammalian Cell Cycle Regulation

*Rajat Singhania, R. Michael Sramkoski,
James W. Jacobberger, and John J. Tyson*

CONTENTS

1.1 Introduction	1
1.2 Methods	4
1.2.1 Simulations	4
1.2.2 Cells, culture, and fixation	7
1.2.3 Immunofluorescence staining, antibodies, flow cytometry	7
1.2.4 Data pre-processing	8
1.3 Discussion	8
1.4 Results	14
1.4.1 Hybrid modeling approach	14
1.4.2 Cyclin distributions in an asynchronous culture	18
1.4.3 Contact inhibition of cultured cells	19
Keywords	21
Supporting Information	21
Acknowledgments	22
Author Contributions	22
References	22

1.1 INTRODUCTION

The timing of DNA synthesis, mitosis, and cell division is regulated by a complex network of biochemical reactions that control the activities of a family of cyclin-dependent kinases. The temporal dynamics of this reaction network is typically modeled by nonlinear differential equations describing the rates of the component reactions. This approach provides exquisite details about molecular regulatory processes but is hampered by the need to estimate realistic values for the many kinetic constants that determine the reaction rates. It is difficult to estimate these kinetic constants from available experimental data. To avoid this problem, modelers often resort to ‘qualitative’ modeling strategies, such as Boolean switching networks, but these models

describe only the coarsest features of cell cycle regulation. In this chapter it describes a hybrid approach that combines the best features of continuous differential equations and discrete Boolean networks. Cyclin abundances are tracked by piecewise linear differential equations for cyclin synthesis and degradation. The cyclin synthesis is regulated by transcription factors whose activities are represented by discrete variables (0 or 1) and likewise for the activities of the ubiquitin-ligating enzyme complexes that govern cyclin degradation. The discrete variables change according to a predetermined sequence, with the times between transitions determined in part by cyclin accumulation and degradation and as well by exponentially distributed random variables. The model is evaluated in terms of flow cytometry measurements of cyclin proteins in asynchronous populations of human cell lines. The few kinetic constants in the model are easily estimated from the experimental data. Using this hybrid approach, modelers can quickly create quantitatively accurate, computational models of protein regulatory networks in cells.

The physiological behaviors of cells (growth and division, differentiation, movement, death, etc.) are controlled by complex networks of interacting genes and proteins, and a fundamental goal of computational cell biology is to develop dynamical models of these regulatory networks that are realistic, accurate and predictive. Historically, these models have divided along two basic lines: deterministic or stochastic, and continuous or discrete; with scattered efforts to develop hybrid approaches that bridge these divides. Using the cell cycle control system in eukaryotes as an example, we propose a hybrid approach that combines a continuous representation of slowly changing protein concentrations with a discrete representation of components that switch rapidly between ‘on’ and ‘off’ states, and that combines the deterministic causality of network interactions with the stochastic uncertainty of random events. The hybrid approach can be easily tailored to the available knowledge of control systems, and it provides both qualitative and quantitative results that can be compared to experimental data to test the accuracy and predictive power of the model.

The cell division cycle is the fundamental physiological process by which cells grow, replicate, and divide into two daughter cells that receive all the information (genes) and machinery (proteins, organelles, etc.) necessary to repeat the process under suitable conditions [1]. This cycle of growth and division underlies all biological expansion, development, and reproduction. It is highly regulated to promote genetic fidelity and meet the demands of an organism for new cells. Altered systems of cell cycle control are root causes of many severe health problems, such as cancer and birth defects.

In eukaryotic cells, the processes of DNA replication and nuclear/cell division occur sequentially in distinct phases (S and M) separated by two gaps (G1 and G2). The mitosis (M phase) is further subdivided into stages: prophase (chromatin condensation, spindle formation, and nuclear envelope breakdown), prometaphase (chromosome attachment and congression), metaphase (chromosome residence at the mid-plane of the spindle), anaphase (sister chromatid separation and movement to opposite poles of the spindle), telophase (re-formation of the nuclear envelopes), and cytokinesis (cell division). The G1 phase is subdivided into uncommitted and committed sub-phases, often referred to as G1-pm (postmitotic interval) and G1-ps (pre S phase interval), separated

by the ‘restriction point’ [2]. In this chapter, it is referred as the sub-phases G1-pm and G1-ps as ‘G1a’ and ‘G1b’ respectively.

The progression through the correct sequence of cell-cycle events is governed by a set of cyclin-dependent kinases (Cdk’s), whose activities rise and fall during the cell cycle as determined by a complex molecular regulatory network. For example, cyclin synthesis and degradation are controlled, respectively, by transcription factors and ubiquitin-ligating complexes whose activities are, in turn, regulated by cyclin/Cdk complexes.

Current models of the Cdk control system can be classified as either continuous or discrete. Continuous models track the changes of protein concentrations, $C_j(t)$ for $j = 1, 2, \dots, N$, by solving a set of nonlinear ordinary differential equations (ODEs) of the form:

$$\frac{dC_j}{dt} = \sum_{r=1}^R v_{jr} \rho_r (C_1, C_2, \dots, C_N) \quad (1)$$

where ρ_r is the rate of the r^{th} reaction and v_{jr} is the stoichiometric coefficient of species i in reaction r . To each rate term is associated one or more kinetic constants that determine exactly how fast the reaction proceeds under specific conditions. These kinetic constants must be estimated from experimental data, and often there is insufficient kinetic data to determine their values. Nonetheless, continuous models, based on rate equations, have been used successfully to account for the properties of cell proliferation in a variety of cell types: yeast [3-5], fruit fly [6], frog egg [7-8], and cultured mammalian cells [9-11]. They have also proved successful in predicting novel cell-cycle characteristics [12-13].

Discrete models, on the contrary, represent the state of each regulatory protein as $B_j(\tau) = 0$ or 1 (inactive or active), and the state variables update from one discrete time step to the next ($\tau = 0, 1, 2, \dots = \text{ticks of a metronome}$) according to the rule:

$$B_j(\tau + 1) = \Psi_j(B_1(\tau), B_2(\tau), \dots, B_n(\tau)) \quad (2)$$

where $\Psi_j(\dots)$ is a Boolean function (i.e., it equates to either 0 or 1) determined by the topology of the reaction network. For Boolean networks (BNs) there is no notion of reaction ‘rate’ and, hence, no need to estimate kinetic constants. The BN models of the Cdk regulatory network have been proposed for yeast cells [14,15] and for mammalian cells [16]. They have been used to study notions of ‘robustness’ of the cell cycle, but they have not been compared in detail to quantitative properties of cell cycle progression, and they have not been used as predictive tools.

In this chapter it is proposed to combine the strengths of both continuous and discrete modeling, while avoiding the weaknesses of each. The ‘hybrid’ model is inspired by the work of Li et al. [14], who proposed a BN for cell cycle controls. Their model employs 11 state variables that move around in a space of $2^{11} = 2048$ possible states.

Quite remarkably they found that 1764 of these states converge quickly onto a ‘super highway’ of 13 consecutive states that represent a typical cell cycle trajectory (G1b—S—G2—M—G1a). The results of Li et al. indicate that the cell cycle control network is ‘robustly designed’ in the sense that even quite large perturbations away from the usual sequence of cell cycle states are quickly restored to the super highway. In the model of Li et al., G1a is a stable steady state; they do not address the signals that drive cells past the restriction point (the G1a-to-G1b transition).

Despite their intuitive appeal, Boolean models have severe limitations. First of all, metronomic time in BN’s is unrelated to clock time in the laboratory, so Boolean models cannot be compared to even the most basic observations of time spent by cells in the four phases of the division cycle [1]. Also, these models do not incorporate cell size, so they cannot address the evident importance of cell growth in driving events of the cell cycle [17-19]. Lastly, cyclins are treated as either absent or present (0 or 1), so Boolean models cannot simulate the continuous accumulation and removal of cyclin molecules at different stages of the cell cycle [20].

The goal is to retain the elegance of the Boolean representation of the switching network, while introducing continuous variables for cell size, cell age, and cyclin composition, in order to create a model that can be compared in quantitative detail to experimental measurements with a minimal number of kinetic parameters that must be estimated from the data. To this end, to keep the cyclin regulators as Boolean variables but model the cyclins themselves as continuous concentrations that increase and decrease due to synthesis and degradation. Next, replace the Boolean model’s metronome with real clock time to account for realistic rates of cyclin synthesis and degradation, and for stochastic variability in the time spent in each Boolean state of the model. Finally, it introduced a cell size variable, $M(t)$, which affects progression through late G1 phase. The $M(t)$ increases exponentially with time as the cell grows and decreases by a factor of ~ 2 when the cell divides. (The assumption of exponential growth is not crucial; similar results are obtained assuming linear growth between cell birth and division.)

Since the pioneering work of Leon Glass [21,22], hybrid (discrete-continuous) models have been employed by systems biologists in a variety of forms and contexts [23-25]. Engineers have been modeling hybrid control systems for many years [26-28], and they have created powerful simulation packages for such systems [29]: SIMULINK [28], SHIFT [30-31] and CHARON [32], to name a few. It has not used these simulation packages because model can be solved analytically.

1.2 METHODS

1.2.1 Simulations

It simulate a flow cytometry experiment with hybrid model in two steps.

Step 1: Creating complete ‘life histories’ for thousands of cells. At the start of the simulation, we specify initial conditions at the beginning of the cycle (State 1) for a progenitor cell. It used the following initial values of the state variables: $[CycA] = [CycB] = [CycE] = 1$ and $M = 3$. The strategy is to follow this cell through its cycle until it divides into two daughters. Then choose one of the two daughters at random and repeat the process, continuing for 32,500 iterations. The first 500 cells discard,

and keep a sample of 32,000 cells that have completed a replication-division cycle according to our model. In the second step, create a simulated sample of 32,000 cells chosen at random phases of the cell cycle, to represent the cells that were assayed by the flow cytometer.

Let us consider cell i ($1 < i < 32500$) at the time of its birth, t_{i0} . By definition, this cell is in State 1, and assume that know its birth mass, $M(t_{i0})$, and its starting concentrations of cyclins A, B and E. Denote the starting concentrations as $[\text{CycA}(t_{i0})]$, $[\text{CycB}(t_{i0})]$, $[\text{CycE}(t_{i0})]$. In the ensuing discussion, unless it is necessary for clarity, drop the i subscript, it being understood that are talking about a representative cell in the population. It will follow this cell until it divides to produce a daughter cell with known concentrations of cyclins.

According to Table 1, a cell in State 1 has no special conditions to satisfy before moving to State 2. Hence the residence time in State 1 is a random number T_1^T chosen from an exponential distribution with mean $\lambda_1 = 2$ h. The cell enters State 2 at $t_1 = t_0 + T_1^T$. Assuming exponential growth, its size at this time is $M(t_1) = M(t_0) \exp\{\gamma(t_1 - t_0)\} = M(t_0) \exp\{\gamma A_1\}$, where γ is the specific growth rate of the culture and $A_1 = t_1 - t_0$ is the age of the cell when it exits State 1. To illustrate how cyclin concentrations are computed at $t = t_1$, let us consider cyclin A as an example. During the interval $t_0 < t < t_1$, $[\text{CycA}]$ satisfies a linear ODE with effective rate constants $k_{sa1} = k'_{sa} = 5$ and $k_{da1} = k'_{da} + k'''_{da} = 1.4$, because $B_{\text{TfE}} = B_{\text{TfB}} = B_{\text{Cdc20A}} = 0$ and $B_{\text{Cdh1}} = 1$ for a cell in State 1. It can compute the concentration of cyclin A at any time during this interval from

$$[\text{CycA}(t)] = \frac{k_{sa1}}{k_{da1}} + \left([\text{CycA}(t_0)] - \frac{k_{sa1}}{k_{da1}} \right) e^{-k_{da1}(t-t_0)}, t_0 \leq t \leq t_1 \quad (3)$$

Setting $t = t_1$ in this equation gives the number we seek. In this fashion, to start tabulating the following information for each simulated cell:

Time	t_0	t_1	t_2	...
Enter State	1	2	3	...
Age	0	$A_1 = t_1 - t_0$	$A_2 = t_2 - t_0$...
Size	$M(t_0)$	$M(t_1)$	$M(t_2)$...
Cyclin A	$[\text{CycA}(t_0)]$	$[\text{CycA}(t_1)]$	$[\text{CycA}(t_2)]$...
Cyclin B	$[\text{CycB}(t_0)]$	$[\text{CycB}(t_1)]$	$[\text{CycB}(t_2)]$...
Cyclin E	$[\text{CycE}(t_0)]$	$[\text{CycE}(t_1)]$	$[\text{CycE}(t_2)]$...

Notice that, at $t = t_1$ when the cell enters State 2, the transcription factor (TFE) for cyclins E and A turns on, and these cyclins start to accumulate. The cell cannot leave State 2 until cyclin E accumulates to a sufficiently high level: $[\text{CycE}](t) \cdot M(t) = \theta_E$, according to Table 1. When this condition is satisfied, the cell leaves State 2 and enters State 3. The size dependence on this transition is a way to couple cell growth to the

DNA replication-division cycle. According to the parameter settings in Table 1, there is no stochastic component to the transition out of State 2.

To continue in this fashion until the cell leaves State 9 and returns to State 1, when cyclin B is degraded at the end of mitosis. This is the signal for cell division. The age of the cell at division is $A_9 = t_9 - t_0$, and the mass of the cell at division is $M(t_9) = M(t_0) \exp(\gamma \cdot A_9)$. The mass of the daughter cell at the beginning of her life history is $M_{\text{daughter}}(t_0) = \delta \cdot M_{\text{mother}}(t_9)$, where δ is a random number sampled from a normal distribution of mean 0.5 and standard deviation 0.0167 to allow for asymmetries of cell division.

Notice that simulating the life history of a single cell only requires generating about a dozen random numbers and performing a handful of algebraic calculations. At no point do we need to solve differential equations numerically. Hence, one can quickly calculate the life histories of tens of thousands of cells.

Step 2: Finding the DNA and cyclin levels of each cell in an asynchronous sample. In the flow cytometry experiments of Yan et al. [42], a random sample of cells is taken from an asynchronous population, the cells are fixed and stained, and then run one-by-one through laser beams where fluorescence measurements are made. So each data point consists of measurements of light scatter (related to cell size) and fluorescence proportional to DNA and cyclin content for a single cell taken at some random point in the cell cycle. To simulate this experiment we must assign to each of 32,000 simulated cells a number φ_i selected randomly from the interval [0,1], where φ_i refers to the fraction of the cell cycle completed by cell i when it was fixed and stained for measurement. Because, each mother cell divides into two daughter cells, the density of cells at birth, $\varphi = 0$, is twice the density of cells at division, $\varphi = 1$. The ‘ideal’ probability density for an asynchronous population of cells expanding exponentially in number is

$$f(\varphi) = (\ln 2) \times 2^{1-\varphi} \quad (4)$$

According to the ‘transformation method’ [47, Chapter 7.2], to compute φ as

$$\varphi = \log_2 \left(\frac{2}{2-r} \right) \quad (5)$$

where r is a random number chosen from a uniform distribution on [0,1]. In this way, to generate 32,000 fractions, φ_i .

If φ_i is the cell-cycle location of the i^{th} cell when it is selected for the flow cytometry measurements, then its age at the time of selection is $a_i = \varphi_i \cdot A_{i9}$, where A_{i9} is the age of the i^{th} cell at division. Given a value for a_i , we then find the state n ($= 1, 2, \dots$ or 9) of the i^{th} cell at the time of its selection:

$$t_{i,n-1} \leq t_{i0} + a_i < t_{i,n} \quad (6)$$

where $t_{i,n}$ (as defined above) is the time at which the i^{th} cell left state n to enter state $n+1$.

Once to know the state n of the cell, one can compute the concentration of each cyclin in the cell at its exact age a_i by analogy to Eq. (3):

$$[\text{CycA}(a_i)] = \frac{k_{sa,n}}{k_{da,n}} + \left([\text{CycA}(t_{i,n-1})] - \frac{k_{sa,n}}{k_{da,n}} \right) e^{-k_{da,n}(t_{i0}+a_i-t_{i,n-1})} \quad (7)$$

where $k_{sa,n}$ and $k_{da,n}$ are the synthesis and degradation rate constants for cyclin A in state n . This is a straightforward calculation because in Step 1 stored the values of t_n and $[\text{CycA}(t_n)]$ for every state of each cell. It can also calculate the mass of cell i at the time of its selection:

$$M(a_i) = M(t_{i0}) \cdot \exp(\gamma \cdot a_i) \quad (8)$$

where $M(t_{i0})$ is the mass at birth of cell i and γ is the specific growth rate of the culture. Because the flow cytometer measures the total amount of fluorescence proportional to all cyclin A molecules in the i^{th} cell, we take as our measurable the product of $[\text{CycA}(a_i)]$ times $M(a_i)$.

Lastly, to determine the DNA content of cell i at age a_i according to:

1. DNA = 1 for $t_{i0} \leq t_{i0} + a_i < t_{i3}$ = entry of i^{th} cell into S phase
2. DNA = $1 + (t_{i0} + a_i - t_{i3}) / (t_{i4} - t_{i3})$ for $t_{i3} \leq t_{i0} + a_i < t_{i4}$ = exit of i^{th} cell from S phase
3. DNA = 2 for $t_{i4} \leq t_{i0} + a_i < t_{i9}$

Now, one simulated values for the measurable quantities of each cell at the time point in the cell cycle when it was selected for analysis. Before, plotting these numbers, one should take into account experimental errors, such as probe quality, fixation, staining and measurement. To do so by multiplying each measurable quantity (DNA content and cyclin levels) by a random number chosen from a Gaussian distribution with mean 1 and standard deviation = 0.03 for DNA measurements and 0.15 for cyclin measurements. These choices give scatter to the simulated data that is comparable to the scatter in the experimental data.

1.2.2 Cells, Culture, and Fixation

Culture and fixation of RKO cells were described [42]. The immortalized HUVEC cells [48] at passage 93 were seeded at 2.5×10^3 cells/cm² in 10 ml EGM-2 media with 2% fetal bovine serum (Lonza, Basel). Duplicate plates were prepared for each time point at days 1, 2, 3, 4, 5, 6, 7, 10, and 15. The cells were fed every other day by replacing half the volume of used media. At the indicated times, cells were trypsinized, washed, and cell counts performed with a Guava Personal Cytometer (Millipore, Billerica, MA). Fixation was as previously described [49]; briefly, cells were treated with 0.125% formaldehyde (Polysciences, Warrington, PA) for 10 min at 37°C, washed, then dehydrated with 90% Methanol. Cells were fixed in aliquots of 1×10^6 cells (days 1–3) or 2×10^6 (days 4–15). Fixed cell samples were stored at -20°C until staining for cytometry.

1.2.3 Immunofluorescence Staining, Antibodies, Flow Cytometry

Staining and cytometry for RKO cells were described [42]. Briefly, cells were trypsinized, fixed with 90% MeOH, washed with phosphate buffered saline, then stained with

monoclonal antibodies reactive with cyclin B1, cyclin A, phospho-S10-histone H3, and with 4',6-diamidino-2-phenylindole (DAPI). For a detailed, updated version of antibodies, staining, and cytometry for cyclins A2 and B1, phospho-S10-histone H3, and DNA content, see Jacobberger et al. (38).

1.2.4 Data Pre-Processing

Data pre-processing was performed with WinList (Verity Software House, Topsham, ME). Doublet discrimination (peak versus area DAPI plot) was used to limit the analysis to singlet cells; non-specific binding was used to remove background fluorescence from the total fluorescence related to cyclin A2 and B1 staining. The phycoerythrin channel (cyclin A2) was compensated for spectral overlap from FITC or Alexa Fluor 488. For simplification, very large 2C G1 HUVEC cells and any cells cycling at 4C→8C were removed from the analysis. These were present at low frequency.

1.3 DISCUSSION

It had constructed a simple, effective model of the cyclin-dependent kinase control system in mammalian cells and used the model to simulate faithfully the accumulation and degradation of cyclin proteins during asynchronous proliferation of RKO (colon carcinoma) cells. The model is inspired by the work of Li et al. [14], who proposed a robust Boolean model of cell cycle regulation in budding yeast. The goal was to retain the elegance of the Boolean representation of the switching network, while introducing continuous variables for cell size, cell age, and cyclin composition, in order to create a model that could be compared in quantitative detail to experimental measurements.

It was shown that this model can accurately simulate flow-cytometric measurements of cyclin abundances in asynchronous populations of growing-dividing mammalian cells. The parameters in the model that allow for a quantitative description of the experimental measurements are easily estimated from the data itself. Now that the model is parameterized and validated for wild-type cells, are currently extending it to handle the behavior of cell populations perturbed by drugs and by genetic interference. In some cases, only modest extensions of the model are required; in other cases, a more thorough overhaul of the way the discrete and continuous variables interact with each other is necessary.

To choose parameter values in model to capture the major features of cyclin fluctuations as measured by flow cytometry during the somatic division cycle of mammalian cells. A human tumor cell line used to calibrate model. Between cell lines and normal human cultured cells, there are differences in the expressions of A and B cyclins [43]; however, when the levels of cyclin B1 were rigorously compared for HeLa, K562, and RKO cells, both the patterns and magnitudes of expression are remarkably similar, apparently dependent to some degree on the rate of population growth [44]. In addition, the patterns of expression of cyclins A2 and B1 are similar for these human tumor cell lines and stimulated normal human circulating lymphocytes (Supporting Fig. S2). Overall, the simulation outputs have satisfying similarity both in pattern and magnitude to the real data for RKO cells, and simulated expression patterns of cyclins A, B and E for the tumor cell line are quite similar to the simulated expression patterns in HUVEC cells (see Supporting Fig. S1).